International Journal of Environmental Science and Technology (2022) 19:6345–6358
https://doi.org/10.1007/s13762-021-03563-0

ORIGINAL PAPER

The mechanisms and kinetics of phosphate adsorption onto iron-coated waste mussel shell observed from hydrodynamic column

M. A. Fulazzaky[1,2] · N. A. A. Salim[3] · M. H. Khamidun[4] · M. H. Puteh[3,5] · A. R. M. Yusoff[6] · N. H. Abdullah[7] · A. Syafiuddin[8] · M. A. A. Zaini[9]

Received: 8 January 2021 / Revised: 18 June 2021 / Accepted: 18 July 2021 / Published online: 23 July 2021

Abstract

The excessive amount of phosphate in domestic wastewater treatment plant effluent must be removed to protect the natural environment of healthy aquatic ecosystem. Though a number of adsorption techniques with various low-cost adsorbent have been proposed, it is still ambiguous how the iron-coated waste mussel shell properties affect the adsorption kinetics of phosphate removal from an effluent. The analysis of experimental data was carried out using the bed depth service time, Thomas, and modified mass transfer factor models to study the adsorption kinetics of phosphate deposited on the surface of iron-coated waste mussel shell observed from hybrid plug flow column reactor. The overall adsorption kinetics of phosphate investigated using the K_a and N_o values referred to the bed depth service time models and the K_T and q_o values referred to the Thomas models are still acceptable. Detailed analysis of the mechanisms of film mass transfer and porous diffusion using the modified mass transfer factor models is able to determine the kinetic rate of phosphate adsorption. Mass transfer resistance for the adsorption of phosphate onto iron-coated waste mussel shell from domestic wastewater treatment plant effluent is dependent on porous diffusion ultimately contributing to develop advanced iron-coated waste mussel shell adsorbent for enhancing the performance of hybrid plug flow column reactor in future.

Keywords Adsorption kinetic model · Domestic wastewater treatment plant effluent · Film mass transfer · Hybrid plug flow column reactor · Phosphate · Porous diffusion

Editorial responsibility: Lifeng Yin.

✉ M. A. Fulazzaky
mohamad.ali.fulazzaky@tdtu.edu.vn

[1] Environmental Engineering and Management Research Group, Ton Duc Thang University, No.19, Nguyen Huu Tho Street, Tan Phong Ward, District 7, Ho Chi Minh City 758307, Vietnam

[2] Faculty of Environment and Labour Safety, Ton Duc Thang University, No.19, Nguyen Huu Tho Street, Tan Phong Ward, District 7, Ho Chi Minh City 758307, Vietnam

[3] Faculty of Engineering, School of Civil Engineering, Universiti Teknologi Malaysia (UTM), 81310 Skudai, Johor Bahru, Johor, Malaysia

[4] Faculty of Civil and Environmental Engineering, Universiti Tun Hussein Onn Malaysia, 86400 Parit Raja, Batu Pahat, Johor, Malaysia

[5] Centre for Environmental Sustainability and Water Security, Research Institute for Sustainable Environment, Universiti Teknologi Malaysia (UTM), 81310 Skudai, Johor Bahru, Johor, Malaysia

[6] Faculty of Science, Universiti Teknologi Malaysia (UTM), 81310 Skudai, Johor Bahru, Johor, Malaysia

[7] Faculty of Civil Engineering, Centre for Diploma Studies, Universiti Tun Hussein Onn Malaysia, 84600 Muar, Johor, Malaysia

[8] Department of Public Health, Faculty of Health, Universitas Nahdlatul Ulama Surabaya, Jalan Raya Jemursari No.57, Jemur Wonosari, Surabaya 60237, Indonesia

[9] Faculty of Engineering, School of Chemical and Energy Engineering, Universiti Teknologi Malaysia (UTM), 81310 Skudai, Johor Bahru, Johor, Malaysia

Introduction

Even though the water quality parameters of pH, dissolved oxygen (DO), biochemical oxygen demand (BOD), chemical oxygen demand (COD), and ammonium (NH_4^+) have been regularly monitored for domestic wastewater treatment plant effluent (DWTPE) in many developed countries, the monitoring of soluble and total phosphorus is not common in Malaysia, but it is valuable. An excessive amount of phosphate (PO_4^{3-}) in the aquatic environment can lead to an increased growth of algae and other aquatic plants (Wu et al. 2019), which can result in a decreased level of DO in the water leading to depopulate the aquatic life and deteriorate the quality of water (Li et al. 2016). The acceptable limits of phosphorus discharged into the surface waters have been regulated by the United States Environmental Protection Agency (USEPA), the European Union (EU) Wastewater Directive, and the Malaysia Environmental Quality for Sewage Regulations 2009. The application of effluent quality standards regulated by the law is a vital requirement to protect the environment for better public health. In spite of the USEPA permits the total phosphorus (TP) concentration of less than 0.8 mg L^{-1} in an effluent and the effluent limit of TP regulated by the EU Wastewater Directive is 2 mg L^{-1} for an agglomeration with population equivalent of 10,000–100,000 (Fulazzaky et al. 2014a), the Malaysian effluent standards can tolerate the amount of TP in effluent up to 5 mg L^{-1} (Sabeen et al. 2018; Osman et al. 2020). This argues that higher concentration of TP permitted by the Malaysian effluent standards makes the operators of wastewater treatment plant less sensitive to an eutrophication of the aquatic environment. The limit of environmentally realistic TP concentration regulated by the Malaysian Environmental Quality Act is required to avoid the eutrophication of water body in Malaysia.

Various methods of the physical, chemical and biological processes have been proposed for the removal of PO_4^{3-} from an effluent. Using the biological method may achieve a high efficiency of PO_4^{3-} removal, but it has several types of variables to be controlled to ensure an optimum performance of the treatment process (Bali and Gueddari 2019; Nagoya et al. 2019). The application of chemical method requires an additional cost of chemical usage in the wastewater treatment system (Lalley et al. 2016). The combination of biological and chemical processes can allow to protect the eutrophication of receiving water from phosphorus pollution while saving on P-sludge disposal costs (Tomei et al. 2020), but it is still complicated and expensive. Among all these purification methods, adsorption is a promising and attractive method of PO_4^{3-} removal from effluent due to the adsorption process may gain popularity for the reasons of operational simplicity and cost effectiveness, while the possibility of producing secondary pollutant is minimal (De Gisi et al. 2016; Zhang et al. 2019). The use of the renewable resource-based iron oxides nanocomposites could be useful for the removal of PO_4^{3-} from contaminated waters (Nakarmi et al. 2019). The application of sand and eggshell coated with iron has been proposed as a favorable and low-cost adsorbent for the removal of PO_4^{3-} from wastewater (Mezenner and Bensmaili 2009; Liu et al. 2018), but the potential of waste mussel shell coated with iron as a potential adsorbent to remove PO_4^{3-} from effluent has not been investigated yet.

The applicability of the various adsorption models has been assessed for the removal of PO_4^{3-} from the waters by different adsorbents (Abou Nohra et al. 2007; Mekonnen et al. 2020). The various adsorption isotherm and kinetic models have been proposed to describe the behaviors of adsorbate–adsorbent interactions (Jung et al. 2015; Riahi et al. 2017; Syafiuddin et al. 2018). Even though many physical and mathematical models have been proposed to study the behavioral kinetics of PO_4^{3-} adsorption (Kumar et al. 2010; Song et al. 2011; Bunce et al. 2018; Silva et al. 2020), the application and validity of the kinetic models to describe the behaviors of PO_4^{3-} adsorption onto the iron-coated waste mussel shell (ICWMS) are still not fully understood. The adsorption isotherm and kinetics of the PO_4^{3-} removal have been studied using the batch-adsorption techniques to provide better understanding on the feasibility of ICWMS used as the potential adsorbent material (Abdul Salim et al. 2021). However, the investigation of PO_4^{3-} removal by the ICWMS material is still required to understand the behavioral kinetics of column adsorption. The objectives of this study are: (1) to investigate the applicability of the bed depth service time (BDST), Thomas, and modified mass transfer factor (MMTF) models for describing the mechanisms of PO_4^{3-} adsorption onto ICWMS from domestic wastewater treatment plant effluent (DWTPE) and (2) to determine the resistance of mass transfer, which is dependent on either film mass transfer (FMT) or porous diffusion (PD), to provide a better understanding on the behavioral kinetics of PO_4^{3-} adsorption onto ICWMS from DWTPE in hydrodynamic column. The column experiments using the hybrid plug flow column reactor (HPFCR) were performed at the Laboratory of Center for Environmental Sustainability and Water Security, Research Institute for Sustainable Environment, Universiti Teknologi Malaysia, from 12 November 2017 to 23 May 2018.

Materials and methods

Domestic wastewater treatment plant effluent

Because of the content of PO_4^{3-} is commonly higher than a limit value regulated by the law, the tertiary treatment of DWTPE is required before discharging into a river. This study used the effluent samples of DWTPE collected from the Taman Sri Pulai of Johor Bahru in Malaysia (latitude 1°33′59.1″N and longitude 103°36′56.7″E) to feed the laboratory-scale device of HPFCR treatment system. Characteristics of the DWTPE quality can be classified as a moderate concentration based on an average value of the parameters of PO_4^{3-}, NH_4^+, NO_3^-, SO_4^{2-}, Cl^-, COD, SS, pH, DO, and conductivity monitored during seven months from November 2017 to May 2018 (see Table 1). The fickle nature of weather patterns in a tropical region could be not related to the quality of DWTPE released into the receiving environment (Misra 2014). The adsorption of PO_4^{3-} onto ICWMS from DWTPE aimed to allow the design characterization of HPFCR treatment system and to describe the kinetic behaviors of PO_4^{3-} removal.

Fig. 1 The waste mussel shell dumped on the riverbank of kampung Pasir Putch at Pasir Gudang village of Johar state in Malasiya

Adsorbent

Approximately 8-g sample of the waste mussel shell (WMS) was collected from the riverbank area of Kampung Pasir Puteh, Pasir Gudang, in Johor state of Malaysia (see Fig. 1). The WMS sample was washed several times with tap water and then dried in an oven at 30 °C for 48 h. The dried WMS sample was crushed using the mortar crusher and then sieved through the sieve fraction of 1.18 mm and retained

Table 1 Characteristics of DWTPE and PFC dimension used for running experiments

The characteristics of DWTPE collected from Taman Sri Pulai of Johor Bahru				
Parameter	Unit	Concentration		
		Minimum	Average	Maximum
PO_4^{3-}	mg L^{-1}	5.6	7.0	8.4
NH_4^+	mg L^{-1}	7.4	10.2	11.8
NO_3^-	mg L^{-1}	0.1	0.5	1.1
SO_4^{2-}	mg L^{-1}	8.0	12.5	15.0
Cl^-	mg L^{-1}	10.0	18.0	37.5
COD	mg L^{-1}	170.0	180.0	195.0
SS	mg L^{-1}	12.0	31.2	84.0
pH	–	6.6	7.1	7.4
DO	mg L^{-1}	5.1	5.4	5.6
Conductivity	µS cm^{-1}	369.0	383.5	414.0
Dimensions of PFC bed equipped the HPFCR treatment system				
Parameter	Unit	Dimension		
Internal diameter	cm	2.6		
Column height	cm	24		
Average size of ICWMS	mm	0.6		
Volumetric flow rate	L h^{-1}	0.071		
PFC bed depth	cm	3, 5, 7, 10, 13, 16		
Amount of ICWMS in the PFC bed	g	19.0, 33.8, 44.9, 63.1, 79.8, 101.3		

on the 0.60 mm mesh. The mean size of WMS was calculated at around 0.89 mm. The solution of 0.5 M Fe(III) was prepared by dissolving $Fe(NO_3)_3.9H_2O$ into deionized water. Base solution of 5.0 N NaOH was added using the dropper into 100 mL of 0.5 M Fe(III) solution until reaching at pH of 9.5 ± 0.1. Then, 200 g of WMS sample was added into 100 mL of 0.5 M Fe(III) and mixed by agitating on the mechanical shaker at the speed of 160 rpm at room temperature for 24 h to obtain the ICWMS material sample. Then, the sample of ICWMS was washed with tap water until its runoff reaching at pH 7 and then dried at 100 °C for 8 h. The ICWMS material was used as a potential adsorbent for the adsorption of PO_4^{3-} from DWTPE applied in hydrodynamic column.

Experimental device and operational procedure

This study used the HPFCR equipment of combining slow sand filtration (SSF) and plug flow column (PFC) as the laboratory-scale device. The fine sand with an average diameter of 0.6 mm used to fill the SSF bed must be rinsed with tap water to remove as much of the impurities as possible. The SSF process can partially remove the organic and inorganic compounds and filters certain microorganisms depending on the SSF bed depth and flow rate of the DWTPE passing through the HPFCR treatment system. The laboratory-scale HPFCR system consists of 50-L storage tank, perforated acrylic sheet with its round hole diameter of 2 mm, silicon tubes, peristaltic pump, fixed bed ICWMS column, and sampling bottles, as shown in Fig. 2. SSF was filled with fine sands (an average diameter of 0.6 mm) placed on the top, coarse sands (an average diameter of 1.18 mm) in middle, and gravels (an average diameter of 2.2 mm) at the bottom of SSF bed, whereas each layer of the SSF bed has a depth of 0.1 m. The dimension of SSF bed has a cross-sectional area of 0.1×0.3 m^2 and depth of 0.9 m. The PFC bed made up of acrylic glass used for the adsorption of PO_4^{3-} from DWTPE has an inner diameter of 26 mm. The concentrations of PO_4^{3-}, NH_4^+, COD and SS were regularly monitored at inlet in the storage tank, after the SSF bed, and outlet of the HPFCR treatment system. Table 1 shows the design characterization of HPFCR system for the removal of PO_4^{3-} from DWTPE. The experimental period of 192 d aimed to include the dry and rainy seasons in Malaysia was set to reach nearly 100% of the PO_4^{3-} breakthrough.

Analytical methods

The performance of HPFCR was analyzed based on the concentrations of PO_4^{3-}, NH_4^+, COD, and SS monitored at inlet and outlet of the HPFCR treatment system during the experimental period of 192 d. The measurements of PO_4^{3-} by the amino acid method, NH_4^+ by the Nessler method, COD by the COD reactor digestion (HACH DRB200 COD Digester) and spectrophotometric method, and SS by the gravimetric method (APHA 2017) were performed at 3.5, 24, 48, 96, 144, 168 and 192 d of the experiment. The analysis of PO_4^{3-}, NH_4^+, COD was carried out using the HACH DR 6000 UV–Vis Spectrophotometer. The measurements of pH and DO were performed using the portable pH meter (Jenway Model 350 pH meter) and the portable DO meter (Jenway Model 970 DO meter), respectively.

The material of ICWMS was sputtered coating with a thin layer of gold using the SC7620 Mini Sputter Coater (Quorum Technologies Ltd., Lewes East Sussex, UK) for the physical and chemical characterizations. The chemical compositions (in %) of ICWMS material were analyzed using the energy dispersive X-ray fluorescence (EDXRF)

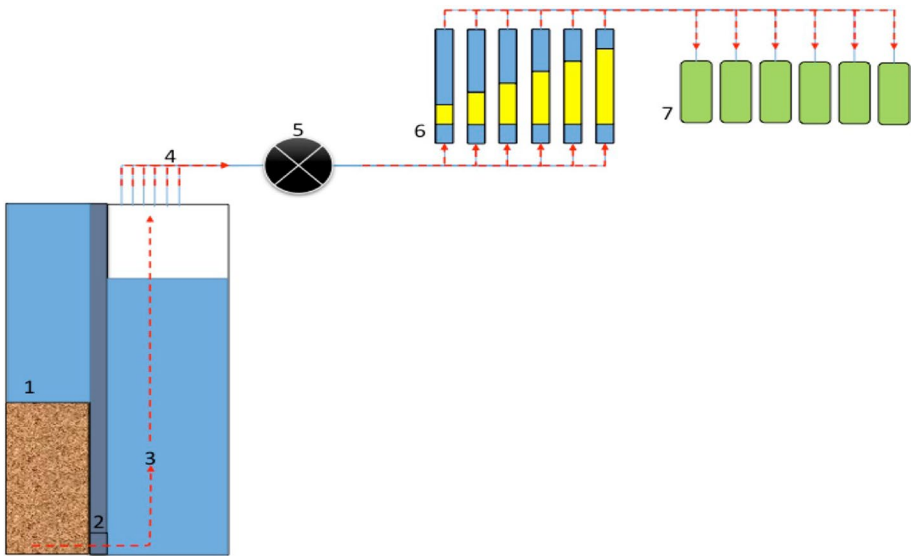

Fig. 2 Schematic of the HPFCR with (1) storing tank, (2) perforated acrylic fleet with a hole diameter of 2 mm, (3) sand filter, (4) silicon tube, (5) peristaltic pump, (6) plug flow columns, and (7) sampling bottles

spectrometer (Rigaku, Sendagaya, Shibuya-Ku, Tokyo, Japan). The Brunauer, Emmett and Teller (BET) surface area of ICWMS material was determined by the multiple-point method using the Surfer Analyser (Thermo Scientific Technologies, Milan, Italy). The characterization of surface morphology of the ICWMS material was performed using the TM3000 Scanning Electron Microscope (SEM) (Hitachi High-Technologies, Naha-shi, Okinawa, Japan). Types of the mineral phases in the ICWMS material were identified using the X-ray diffraction (XRD) analysis of the Bruker D8 Advance High resolution diffractometer.

Numerical simulation and data analysis

Calculation of the HPFCR efficiency

The adsorption capacity of ICWMS used as an adsorbent was assessed from the HPFCR performance to remove the pollutants of PO_4^{3-}, SS, COD, and NH_4^+ from DWTPE. Based on the data of monitoring the PO_4^{3-}, SS, COD, and NH_4^+ concentrations at inlet and outlet of the HPFCR treatment system with a PFC depth of 7 cm, the performance of HPFCR can be calculated using the equation of:

$$E = \frac{C_i - C_e}{C_i} \times 100\% \tag{1}$$

where E is the efficiency of HPFCR to remove either PO_4^{3-}, SS, COD or NH_4^+ from DWTPE (%), C_i is the concentration of either PO_4^{3-}, SS, COD or NH_4^+ at inlet of the HPFCR treatment system (mg L^{-1}) and C_e is the concentration of either PO_4^{3-}, SS, COD or NH_4^+ at outlet of the HPFCR treatment system (mg L^{-1}).

Bed depth service time models

Even though the adsorption behaviors of solutes onto the various materials can be described using several kinetic models (Syafiuddin et al. 2018), this study used the BDST, Thomas, and MMTF models to predict the kinetics of PO_4^{3-} adsorption onto ICWMS from DWTPE because each of these models has a typical underlying assumption in the process modeling. The BDST models originally developed based on the quasi-chemical rate law (Bohart and Adams 1920) can be used to analyze the effect of various operating variables on the performance of ICWMS to remove PO_4^{3-} from DWTPE. However, the dispersion of PO_4^{3-} caused by the mass transfer resistance in film zone surrounding the surface of ICWMS or by the PD within the pores is negligible. The modified BDST models proposed by Hutchins can be written in the form of linear equation (Pember et al. 2016):

$$t = \frac{N_o \times h}{C_o \times v} - \frac{1}{K_a \times C_o} \ln\left(\frac{C_o}{C_s} - 1\right) \tag{2}$$

where t is the service time (h), N_o is the dynamic adsorption capacity per unit volume of the PFC (mg L^{-1}), h is the depth of PFC (cm), C_o is the concentration of PO_4^{3-} entered the PFC (mg L^{-1}), v is the linear flow rate (cm h^{-1}), K_a is the adsorption rate constant (L h^{-1} mg^{-1}), and C_s is the concentration of PO_4^{3-} flowed out of the PFC bed (mg L^{-1}).

By simplifying Eq. (2) can be written in the form of:

$$t = (a \times h) - b \tag{3}$$

with $a = \frac{N_o}{C_o \times v}$ is a constant (in h cm^{-1}) and $b = \frac{1}{K_a \times C_o} \ln\left(\frac{C_o}{C_s} - 1\right)$ (h).

By plotting t versus h provides the graph of linear function with a as the slope and b as the Y-intercept, which can be used to calculate the value of N_o for a given set of the C_o and v values. The variant K_a according to the percentage of PO_4^{3-} breakthrough can be calculated using the equation of:

$$K_a = \frac{1}{b \times C_o} \ln\left(\frac{C_o}{C_s} - 1\right) \tag{4}$$

where a is the retention coefficient relying to the velocity of the PO_4^{3-} passed the PFC bed (h cm^{-1}) and b is the contact time constant relying to the availability of the space and acceptor sites of the ICWMS adsorbent (dimensionless).

Thomas models

The Thomas models developed based on the assumptions that the kinetic process of PO_4^{3-} adsorption onto ICWMS from DWTPE is to follow the adsorption–desorption kinetics of the Langmuir model with no any axial dispersion and no other mass transfer resistances (Ahmed and Hameed 2018). The prediction of concentration–time profile can help achieve a proper design of HPFCR treatment system by simulating the experimental data collected from the PFC depths of 3, 5, 7, 10, 13 and 16 cm and can be used to investigate the PO_4^{3-} content of tracer breakthrough curve. The calculation of equilibrium solute uptake per gram of ICWMS gives an insight on the requirement for the development of HPFCR treatment system to adjust the design parameters. The Thomas models can be written as follows (Khadhri et al. 2019):

$$\frac{C_s}{C_o} = \frac{1}{1 + \exp[K_T(q_o \times m - C_o \times V)/Q]} \tag{5}$$

where K_T is the kinetic coefficient or the Thomas rate constant (L h^{-1} mg^{-1}), q_o is the equilibrium PO_4^{3-} uptake per gram of ICWMS (mg g^{-1}), m is the amount of ICWMS in

the PFC bed (g), V is the effective volume of DWTPE passed the PFC bed (L), and Q is the volumetric flow rate (L h^{-1}).

A simplification of Eq. (5) can be written in the linear equation (Kausar et al. 2017) of:

$$\ln\left(\frac{C_o}{C_s}-1\right)=-(c\times t)+d \tag{6}$$

with $c = K_T$ x C_o as the slope is a constant (h^{-1}), $t=\frac{V}{Q}$ is the service time (h), and $d=\frac{K_T\times q_o\times m}{Q}$ as the Y-intercept is a constant (dimensionless) due to the experiment was set at a constant flow rate.

The values of K_T and q_o can be calculated for a given flow rate if the values of c as the slope and d as the Y-intercept have been verified from the linear graph of $\ln(C_o/C_s—1)$ versus t according to Eq. (6) (Recepoğlu et al. 2018).

Modified mass transfer factor models

The accumulative quantity of PO_4^{3-} deposited on the surface of ICWMS pursuant to the effective volume of DWTPE flowed through the PFC bed can be calculated using the equation (Fulazzaky et al. 2013):

$$q=\int_0^V\frac{(C_o-C_s)dV}{m} \tag{7}$$

where q is the cumulative quantity of PO_4^{3-} deposited on the ICWMS surface at volume V of DWTPE passed the PFC bed (mg g^{-1}).

The MMTF models as the improvement of the mass transfer factor models (Fulazzaky 2011) could be useful to study a competitive effect of coexisting Cl^-, NO_3^- and SO_4^{2-} anions on the kinetics of PO_4^{3-} adsorption onto ICWMS from DWTPE and can be written in the form (Fulazzaky et al. 2013) of:

$$\ln\left(\frac{C_o}{C_s}\right)=[k_La]_g\times e^{-\beta\times\ln(q)}\times t \tag{8}$$

where $[k_La]_g$ is the global mass transfer factor (h^{-1}) and β is the absorbate–adsorbent affinity parameter (g h mg^{-1}).

The simplification of Eq. (8) yielding a linear equation can be mathematically written as:

$$\ln(q)=\frac{1}{\beta}\times\ln(t)+B \tag{9}$$

with

$$B=\frac{\ln\left([k_La]_g\right)-\ln\left\{\ln\left(\frac{C_o}{C_s}\right)\right\}}{\beta} \tag{10}$$

where B is the potential mass transfer index relating to driving force of PO_4^{3-} mass transfer from bulk water to acceptor sites (mg g^{-1}).

A correlation of the external mass transfer factor ($[k_La]_f$) to $[k_La]_g$ can be written in the form (Fulazzaky et al. 2013) of:

$$[k_La]_f=[k_La]_g\times e^{-\beta\times\ln(q)} \tag{11}$$

where $[k_La]_f$ is the external mass transfer factor or film mass transfer factor (h^{-1}).

The values of $1/\beta$ as the slope and B and the Y-intercept according to Eq. (9) can be verified from the graph of plotting $\ln(q)$ versus $\ln(t)$. The variation of $[k_La]_g$ value pursuant to the C_o/C_s ratio can be verified using Eq. (10) and the variation of $[k_La]_f$ value to follow the level of PO_4^{3-} accumulated on the surface of ICWMS can be verified using Eq. (11). The value of $[k_La]_g$ minus $[k_La]_f$ is the value of internal mass transfer factor ($[k_La]_d$), which can be written in the equation (Fulazzaky et al. 2013) of:

$$[k_La]_d=[k_La]_g-[k_La]_f \tag{12}$$

where $[k_La]_d$ is the internal mass transfer factor or porous diffusion factor (h^{-1}).

The variation of $[k_La]_d$ value followed the values of $[k_La]_g$ and $[k_La]_f$ can be verified using Eq. (12) to describe the transport mechanism of PO_4^{3-} moved through the matrix pores and to determine the mass transfer resistance by comparing the variation pattern of $[k_La]_d$ with $[k_La]_f$ for the adsorption of PO_4^{3-} from DWTPE onto the ICWMS adsorbent.

Table 2 Chemical composition of ICWMS material (wt.%) analyzed by the EDXRF spectrometer

CaO	Fe_2O_3	SO_3	MgO	K_2O	Na_2O	P_2O_5
88.0	5.90	0.15	0.10	ND	ND	ND

Remarked that the table shows ND for not detected

Results and discussion

Physical and chemical characteristics of the ICWMS adsorbent

The results (Table 2) of the EDXRF analysis show that the chemical composition of ICWMS material consists of 88% CaO, 5.9% Fe_2O_3, 0.15% SO_3 and 0.1% MgO. It is necessary to identify the presence of other components by the XRD analysis since the ICWMS material should report the amount of all elements to reach at 100%. An analysis using the EDXRF spectrometer shows the major oxides of CaO and Fe_2O_3 and the minor oxides of SO_3 and MgO contained in the ICWMS material. The pore space analysis of using the surfer analyser shows that the granular ICWMS adsorbent has a BET surface area of 0.055 $m^2\ g^{-1}$ and is narrower than the untreated mussel shell powder of 1.120 $m^2\ g^{-1}$ (Wei et al. 2018). Surface morphology of the physical features can be observed from the SEM photographs of ICWMS material with 1500 and 6000 times magnification, as shown in Fig. 3.

The SEM image of Fig. 3a with 1500 times magnification shows that the ICWMS material has a relatively rough and irregular surface structure. The SEM image of Fig. 3b with 6000 times magnification exhibits the small pores like opening at the surface of the ICWMS material. The formation of iron oxide coated WMS material can be observed from the SEM photographs and could be beneficial for the removal of PO_4^{3-} ions from aqueous solution (Boujelben et al. 2008).

The XRD pattern of Fig. 3c indicates the presence of aragonite ($CaCO_3$), CaO and Fe_2O_3 as the major oxides and that of SO_3 and MgO as the minor oxides contained in the ICWMS material. The chemical composition of 5.85% can be referred to the presence of $CaCO_3$ by considering the ICWMS material made up of five components, i.e., CaO, Fe_2O_3, $CaCO_3$, SO_3 and MgO. The presence of $CaCO_3$ in aragonite state and CaO on the surface of ICWMS could be favorable for the adsorption of PO_4^{3-} ions from aqueous solution (Kim et al. 2018; Torit and Phihusut 2019). The surface area and Fe_2O_3 content of the ICWMS adsorbent could be the important feature and have exhibited promising

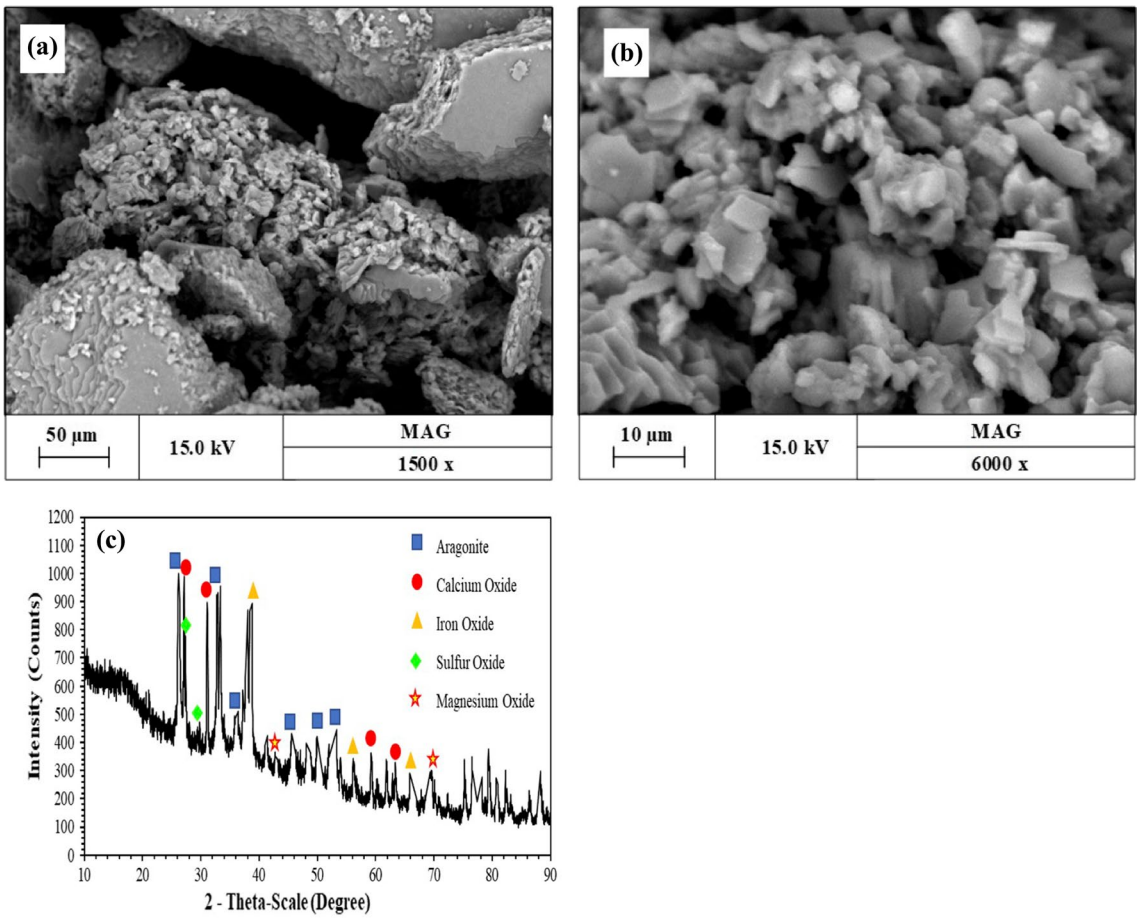

Fig. 3 The characteristics of ICWMS materual observed from **a** SEM image of magnified 1500 times, **b** SEM image if magnified 6000 times and **c** XRD pattern

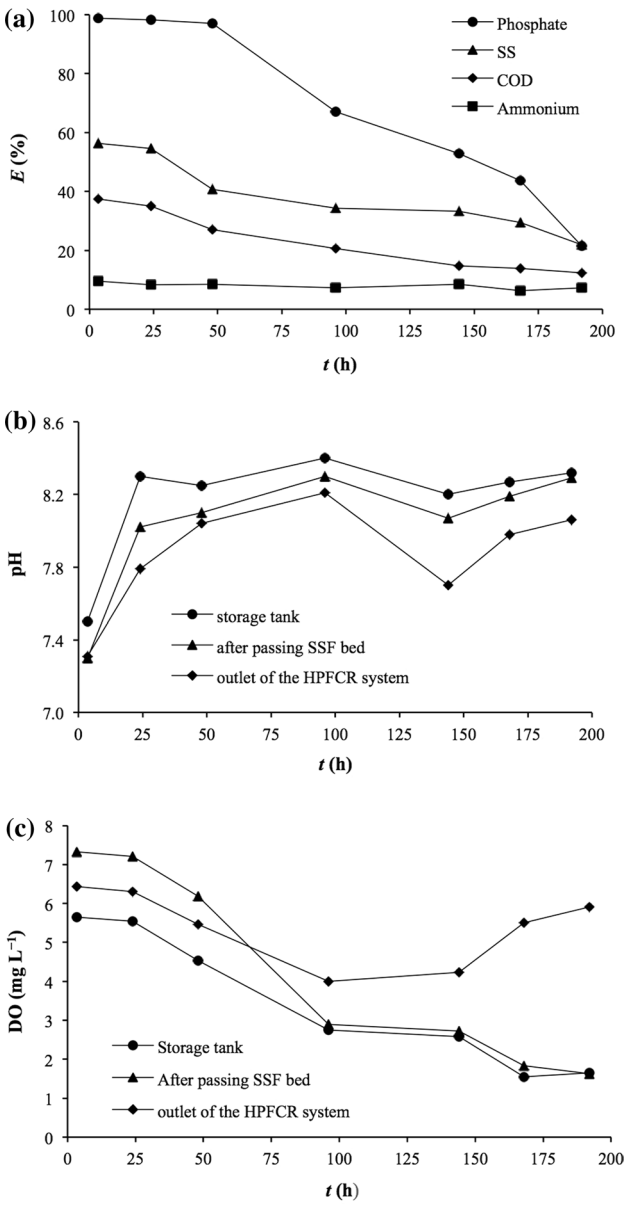

Fig. 4 Varitions of **a** *E*, **b** pH and **c** DO pursuant to *t*

performance for the adsorption of PO_4^{3-} ions from water (de Sousa et al. 2012; Lalley et al. 2016).

Performance of the HPFCR system and its operating conditions

The results (Fig. 4a) show that the removal efficiencies of PO_4^{3-}, SS, COD and NH_4^+ by the HPFCR treatment system monitored at 3.5 h of the experiment can reach 98.7% (see Fig. 4a; line-i), 56.3% (see Fig. 4a; line-ii), 37.5% (see Fig. 4a; line-iii), and 9.5% (see Fig. 4a; line-iv), respectively. A decrease in the performance of HPFCR could be due to the pore space and acceptor sites of the ICWMS adsorbent occupied by the different solutes increase and this can be monitored from an increased breakthrough of the solutes over time during the experiment. The removal efficiency of PO_4^{3-} slightly decreased by 1.7% from 98.7 to 97% monitored after 48 h of the experiment (see Fig. 4a; line-i) could be due to the presence of CaO, Fe_2O_3 and $CaCO_3$ on the surface of ICWMS has a benefit of the positively charged Ca^{2+} and Fe^{3+} ions for the adsorption of negatively charged PO_4^{3-} ions from DWTPE. Then, the performance of HPFCR decreased by 75.1% from 97.0 to 21.9% could be due to the reactive surface of CaO, Fe_2O_3 and $CaCO_3$ occupied by the PO_4^{3-} ions rapidly decreases during the period of 144 h from 48 to 192 h of the experiment. A decrease in the performance of the HPFCR treatment system to remove the mineral and organic pollutants of SS and COD, respectively, could be due to the availability of pore space decreased over time may lead to a significant reduction of the van der Waals force that attracts the mineral and organic matters from DWTPE to the surface of ICWMS (see Fig. 4a; lines-ii, iii). The efficiency of NH_4^+ removed by the HPFCR treatment system has a small fluctuation that ranges from 6.3 to 9.5% (see Fig. 4a; line-iv) and is mainly dependent on the biological process that takes place in the presence of oxygen in DWTPE (Fulazzaky et al. 2018; Karri et al. 2018).

The operating conditions of HPFCR treatment system were investigated by monitoring the variations of pH and DO at inlet in the storage tank, after passing the SSF bed, and outlet in the sampling bottle over time to get better understanding on the characteristic change in the DWTPE. The variations of pH ranged from 7.50 to 8.40 with an average of 8.18 (see Fig. 4b; curve-i) and from 7.30 to 8.30 with an average of 8.04 (see Fig. 4b; curve-ii) were monitored at inlet in the storage tank and after passing the SSF bed, respectively, during the experimental period of 192 h. The pH decreased very slightly could be due to the chemical reaction of fine sand with DWTPE may slightly produce the H^+ ions (Crundwell 2017). The variation of pH monitored at outlet of the HPFCR system ranged from 7.31 to 8.21 with an average of 7.87 (see Fig. 4b, curve-iii) could be due to the presence of Fe_2O_3 in the form of heterolytically dissociated structure on the surface of ICWMS may attract the OH^- ions from solution attached to surface site of Fe^{3+} ions leading to a decreased pH of treated DWTPE (Ovcharenko et al. 2016).

The variation of DO monitored at inlet in the storage tank decreases from 5.65 mg L^{-1} at 3.5 h to 1.65 mg L^{-1} at 192 h of the experiment (see Fig. 4c; curve-i) and that after passing the SSF bed decreases from 7.33 mg L^{-1} at 3.5 h to 1.63 mg L^{-1} at 192 h of the experiment (see Fig. 4c; curve-ii). The DO value of DWTPE monitored after passing the SSF process is remarkably higher than that monitored in the storage tank during the experimental period of 48 h due to the transfer of oxygen from air trapped in fine sands to the water flowing through the SSF bed can lead to increased level of

DO in DWTPE at the beginning of the experiment. The degradation of organic matter occurred during the experiment with the presence of microorganisms in DWTPE can lead to continuously decrease the value of DO monitored from 3.5 to 192 h of the experiment (Passerini et al. 2016). The content of DO monitored at outlet of the HPFCR system decreases from 6.43 mg L^{-1} at 3.5 h to 4.00 mg L^{-1} at 96 h of the experiment (see Fig. 4c; curve-iii) could be due to the bacterial degradation of organic matter with the aid of oxygen can lower the level of DO in the treated DWTPE effluent during the experimental period of 96 h (Le Moigne et al. 2017). An increase in the value of DO from 4.00 mg L^{-1} at 96 h to 5.91 mg L^{-1} at 192 h of the experiment could be due to the diffusion of oxygen in water from the atmosphere may occur when the availability of organic matter in the treated DWTPE effluent is low (Fulazzaky 2013).

Numerical analysis using the bed depth service time models

The dynamic capacity of PO_4^{3-} adsorbed per unit volume of ICWMS and the rate constant of adsorption at certain percentage of PO_4^{3-} out flowing through the various depths of PFC bed can be determined since both the values of a as the slope and b as the Y-intercept have been verified from linear graph of t versus h plotted according to Eq. (3). The correlation between t and h can be made by interpolating the curve of C_s/C_o versus t to determine an actual value of t at 5, 10, 20, 50 and 90% of the PO_4^{3-} breakthrough for the PFC depths of 3, 5, 7, 10, 13 and 16 cm. The plot (Fig. 5a) of t versus h accorded to Eq. (3) yielding the graph of linear function makes the time t to reach at certain percentage of the PO_4^{3-} breakthrough gradually increased with increasing of the PFC depth. Correlation for the parameters a and b is very good ($R^2 > 0.966$, see Table 3); therefore, the use of a and b values could be useful to calculate the values of N_o and K_a. The value of N_o increased from 797 to 805 to 1142 and to 1558 mg L^{-1} is due to the percentage of PO_4^{3-} breakthrough increases from 5 to 10 to 20 and to 50%, respectively (see Table 3). An increase in the value of N_o related to increased amount of PO_4^{3-} deposited on the surface of ICWMS material may not be enough to completely occupy the acceptor sites of CaO, Fe_2O_3 and $CaCO_3$ polymorphs with increasing of the C_s/C_o ratio up to 0.5. The capacity of dynamic PO_4^{3-} adsorption increased with increasing of the C_s/C_o ratio could be due to an increased velocity of the DWTPE flow can lead to an increased force of PO_4^{3-} deposition per unit area of the ICWMS adsorbent (Podder and Majumder 2016). A deep depth of PFC extended life span of the PO_4^{3-} adsorption per unit volume of the ICWMS adsorbent with a maximum capacity of 1558 mg L^{-1} can be achieved at 50% of the C_s/C_o ratio. Physical meaning of the constant K_a can't be clearly understood since an irregular

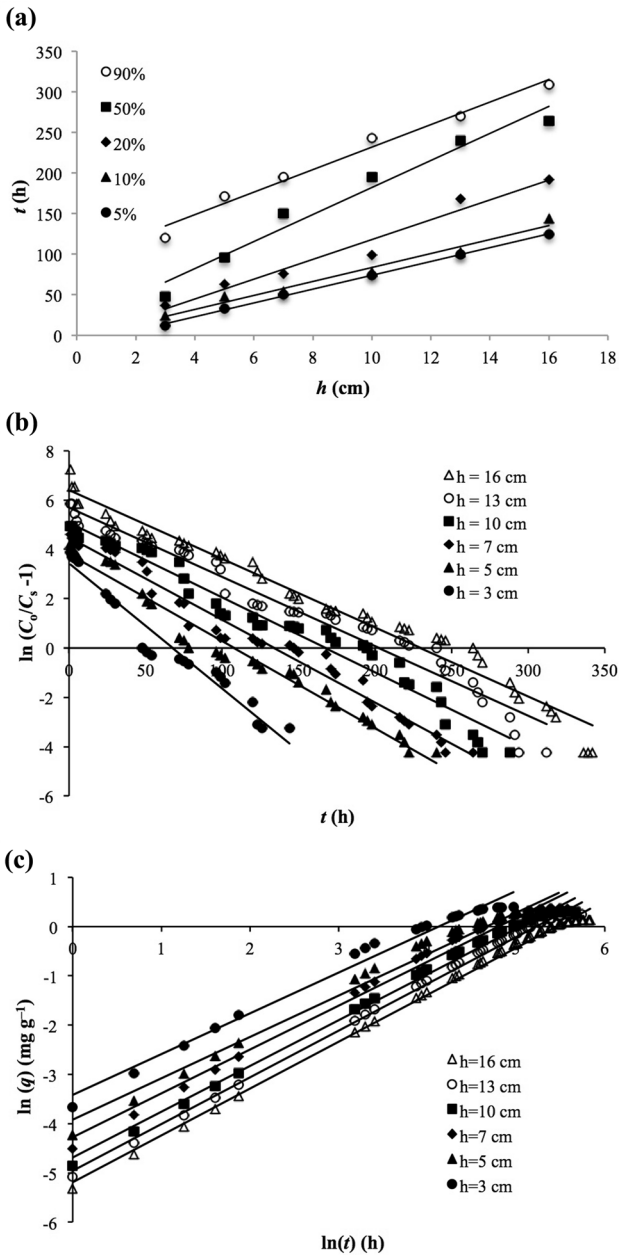

Fig. 5 The linear curves of plotting: **a** t versus h, **b** $\ln(C_o/C_s - 1)$ versus t and **c** $\ln(q)$ versus $\ln(t)$

trend of the K_a variation with increasing of the C_s/C_o ratio (see Table 3) appeared due to the dispersion of PO_4^{3-} caused by the resistance of mass transfer controlled by either film zone surrounding the solid of ICWMS material or PD of PO_4^{3-} inside the pores of ICWMS adsorbent is still negligible. Investigating the kinetic behaviors of FMT and PD for the adsorption of PO_4^{3-} onto ICWMS from DWTPE in hydrodynamic column can gain better understanding of the mechanisms and mass transfer resistance of transporting the PO_4^{3-} ions from bulk water toward the acceptor sites of CaO, Fe_2O_3 and $CaCO_3$ polymorphs.

Table 3 Results of the different parameters calculated using the BDST, Thomas, and MMTF models to describe the adsorption of PO_4^{3-} onto the ICWMS adsorbent

The parameters N_o and K_a calculated using the BDST models					
C_s/C_o (%)	a (h cm^{-1})	b (dimensionless)	N_o (mg L^{-1})	K_a (L h^{-1} mg^{-1})	R^2
5	8.52	− 11.18	797	− 0.0281	0.99877
10	8.61	− 2.46	805	− 0.1276	0.97485
20	12.21	− 4.01	1142	− 0.0485	0.96672
50	16.65	15.67	1558	0.0000	0.96605
90	13.87	93.18	1298	− 0.0034	0.97971
The parameters K_T and q_o calculated using the Thomas models					
h (cm)	m (mg)	K_T (L h^{-1} mg^{-1})	q_o (mg g^{-1})	R^2	
3	19.0	0.0072	1.77	0.95553	
5	33.8	0.0050	1.58	0.97398	
7	44.9	0.0048	1.48	0.97797	
10	63.1	0.0043	1.32	0.96448	
13	79.8	0.0040	1.26	0.96027	
16	101.3	0.0039	1.15	0.97621	
The parameters β and B calculated using the MMTF models					
h (cm)	β (g h mg^{-1})	B (mg g^{-1})	R^2		
3	1.208	− 3.417	0.98290		
5	1.190	− 3.920	0.97658		
7	1.123	− 4.276	0.98641		
10	1.076	− 4.688	0.99286		
13	1.054	− 4.957	0.99558		
16	1.051	− 5.190	0.99527		

Numerical analysis using the Thomas models

The kinetic investigation of PO_4^{3-} adsorption onto the ICWMS adsorbent can be performed based on the analysis of data collected from the experiments run at flow rate of 0.071 L h^{-1} for the various depths of PFC bed using the Thomas models. The plot (Fig. 5b) of $\ln(C_o/C_s—1)$ versus t according to Eq. (6) yields a graph of linear function with the slope marked as c and the Y-intercept as d, which can be used to calculate the values of K_T and q_o. Because of the correlation for the parameters K_T and q_o is very good ($R^2 > 0.9555$; see Table 3), the use of K_T and q_o values could be useful to describe the kinetic behaviors of PO_4^{3-} moved from DWTPE to the surface of ICWMS. The value of K_T decreased from 0.0072 to 0.0050 to 0.0048 to 0.0043 to 0.0040 and to 0.0039 L h^{-1} mg^{-1} and the value of q_o also decreased from 1.77 to 1.58 to 1.48 to 1.32 to 1.26 and to 1.15 mg g^{-1} could be due to an increased depth of the PFC bed from 3 to 5 to 7 to 10 to 13 and to 16 cm, respectively (see Table 3). The collision frequency of PO_4^{3-} ions with the acceptor sites of CaO, Fe_2O_3 and $CaCO_3$ polymorphs decreased with increasing of the granular ICWMS dosage can be verified from a decreased value of K_T for a given flow rate of DWTPE passed across the PFC bed. The distribution of PO_4^{3-} ions spread over the ICWMS adsorbent can expand with an increased amount of ICWMS in the PFC bed and can therefore retain considerable amount of PO_4^{3-} ions deposited on the surface of ICWMS material. The kinetic coefficient K_T decreased with decreasing of the water velocity caused by an increased ICWMS dosage is sensitive to the pore space feature of ICWMS depended on the internal structure and chemical functional groups of the acceptor sites (Ahmed and Hameed 2018; Fulazzaky 2019). The value of q_o decreased with an increase in the PFC depth could be due to the driving force of transporting the PO_4^{3-} ions from the bulk liquid to film zone closely near the solid surface decreases with an increased amount of the ICWMS adsorbent (Charola et al. 2018). Application of the Thomas models for the adsorption of PO_4^{3-} may help explain the collision frequency and driving force of the mass transfer and is related to an external mass transfer of PO_4^{3-} moved from the bulk liquid to a solid surface of the ICWMS adsorbent. The rate of mass transfer controlled by either FMT or PD cannot be predicted from the assessment of the K_T and q_o values. It is

necessary to use a proper kinetic model to determine the mass transfer resistance of PO_4^{3-} adsorption onto ICWMS from DWTPE in the next step of numerical analysis.

Numerical analysis using the modified mass transfer factor models

By plotting ln(q) versus ln(t) according to Eq. (9) yields a graph of linear function with $1/\beta$ as the slope and B as the Y-intercept (see Fig. 5c). Correlation for the parameters β and B is very good ($R^2 > 0.9765$; see Table 3), meaning that the use of the MMTF models could be useful to describe the kinetic behaviors of PO_4^{3-} adsorption onto ICWMS from DWTPE. The results show that both the values of β decreased from 1.208 to 1.190 to 1.123 to 1.076 to 1.054 and to 1.051 g h mg^{-1} and B decreased from − 3.417 to − 3.920 to − 4.276 to − 4.688 to − 4.957 and to − 5.190 mg g^{-1} could be related to an increased depth of PFC bed from 3 to 5 to 7 to 10 to 13 and to 16 cm, respectively (see Table 3). The value of β decreased with increasing of the surface area and pore volume distribution of the ICWMS adsorbent could be due to an increased opportunity of ICWMS attracted coexisting anions of Cl^-, NO_3^- and SO_4^{2-} by the van der Waals force leads to a decreased electronic interaction of PO_4^{3-} with active sites of CaO and Fe_2O_3 (Charola et al. 2018; Afridi et al. 2019). A decrease in the value of B with increased depth of PFC bed is due to the more retention of PO_4^{3-} spread over a large surface area of film zone can reduce the concentration of PO_4^{3-} in the bulk water leading to a decreased driving force of liquid–solid interphase mass transfer (Fulazzaky 2011).

The variation of $[k_La]_g$ calculated using to Eq. (10) is dependent on the C_o/C_s ratio since both the values of β and B have been verified from graphing a linear function. By plotting $[k_La]_g$ versus percent PO_4^{3-} breakthrough (Fig. 6a) shows the pattern of $[k_La]_g$ variation decreased with increasing of the outflow. The GMT of PO_4^{3-} ions transported from the bulk DWTPE to acceptor sites of CaO, Fe_2O_3 and $CaCO_3$ polymorphs decreased with increasing of PO_4^{3-} flowing out of the PFC bed is due to the van der Waals and electrostatic forces decrease with increasing of the pore space occupied by the PO_4^{3-} and coexisting anions. The pattern of $[k_La]_g$ variation progressively lowered with increasing of the PFC depth could be related to the driving force of PO_4^{3-} anions moved toward the reactive surface of Ca^{2+} and Fe^{3+} cations increases with increasing of the movement of DWTPE across the PFC bed (Fulazzaky et al. 2014a). Understanding the mass transfer behaviors of PO_4^{3-} adsorption required more detailed explanation can be gained by investigating the pattern of the $[k_La]_f$ and $[k_La]_d$ variations to determine if the rate of mass transfer is controlled by either FMT or PD.

The variation of $[k_La]_f$ depended on the accumulative amount of PO_4^{3-} deposited on the surface of ICWMS

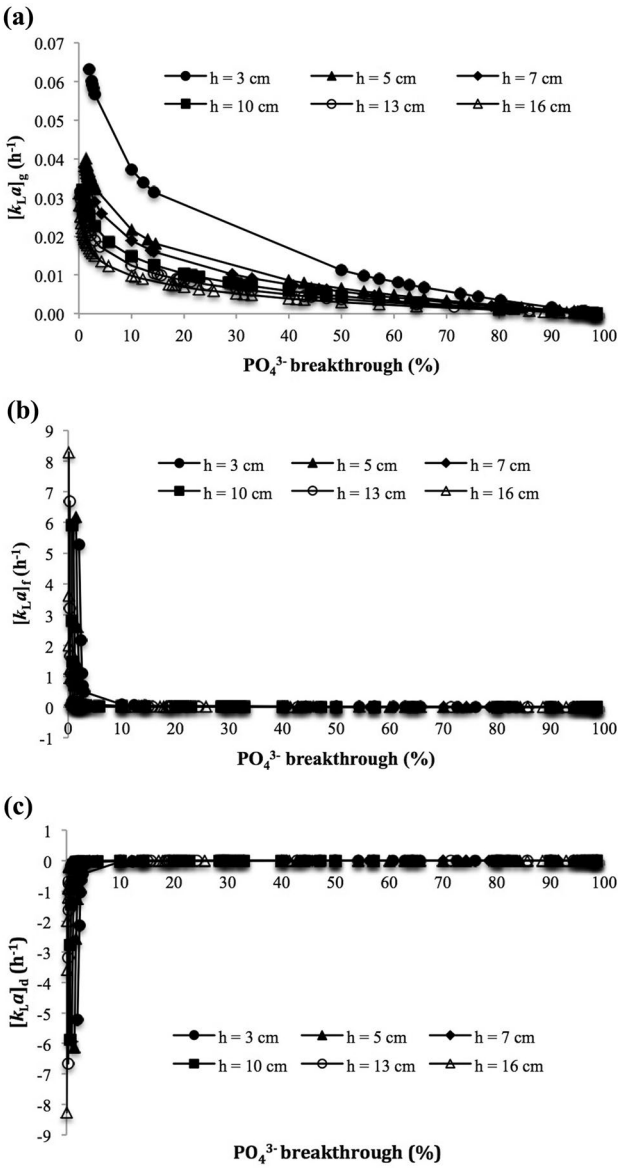

Fig. 6 The variations **a** $[k_La]_g$, **b** $[k_La]_g$, **c** $[k_La]_g$ pursuant to the percentage of PO_4^{3-}

adsorbent can be calculated using Eq. (11) since the value of β verified from straight line graph and the variant $[k_La]_g$ pursuant the C_s/C_0 ratio calculated using Eq. (10) have been obtained. By plotting the curve of $[k_La]_f$ versus percent PO_4^{3-} breakthrough showing the pattern of $[k_La]_f$ variation sharply decreases before reaching at around 5% of PO_4^{3-} flowed out of the PFC bed (see Fig. 6b). High rate of PO_4^{3-} mass transfer moved toward the reactive surface of CaO, Fe_2O_3 and $CaCO_3$ polymorphs could be due to an electronic interaction of the positive Ca^{2+} and Fe^{3+} cations can react with the PO_4^{3-} anions leading to the formation of $Ca_{10}(PO_4)_6(OH)_2$, $Fe_5(OH)_6(PO_4)_3$, Fe–H_2PO_4 or (Fe–)$_2HPO_4$ precipitate, depending on

the environmental conditions of DWTPE solution. The reactions of ion exchange on the surface of ICWMS can be described as follows: (1) $10Ca–CO_3 + 2H^+ + 6HPO_4^{2-} + 2H_2O \rightarrow Ca_{10}(PO_4)_6(OH)_2 + 10HCO_3^-$, (2) $15Fe^{3+} + 9PO_4^{3+} + 18H_2O \rightarrow 3Fe_5(OH)_6(PO_4)_3 + 18H^+$, (3) $Fe–OH + H_2PO_4^- \rightarrow Fe–H_2PO_4 + OH^-$ or (4) $2Fe–OH + HPO_4^{2-} \rightarrow (Fe–)_2HPO_4 + 2OH^-$ (Karageorgiou et al. 2007; Fulazzaky et al. 2014b; Čadež et al. 2018; Liu et al. 2019; Zhong et al. 2019). Chemical reaction of the acceptor sites of the positive Ca^{2+} and Fe^{3+} cations with the PO_4^{3-} anions generates the new chemical bonds at the surface of ICWMS adsorbent. This suggests that the movement of PO_4^{3-} attracted from DWTPE toward the surface of ICWMS mainly dominated by chemisorbed interaction state (Jurado et al. 2021). The depth of chemisorption well within the pores could be a measure of the strength of PO_4^{3-} binding to the ICWMS adsorbent. The modification of WMS surface coated by iron provides a new evidence for the importance of surface functional groups in the chemisorption process (Fulazzaky 2019). The variation (see Fig. 6c) of $[k_La]_d$ used to describe the diffusion behavior of PO_4^{3-} adsorption can be calculated using Eq. (12) since the values of $[k_La]_g$ calculated using Eq. (10) and $[k_La]_f$ calculated using Eq. (11) have been obtained from the data subject. An increase in the value of $[k_La]_d$ varied in the negative zone cannot totally counterbalance the decreasing of the $[k_La]_f$ value varied in the positive zone; hence, the variation of $[k_La]_g$ value is still in the positive zone during the adsorption process. This determines that the resistance of mass transfer controlled the kinetic rate of PO_4^{3-} adsorption onto ICWMS from DWTPE is dependent on PD. The interaction of PO_4^{3-} with the acceptor sites of CaO, Fe_2O_3 and $CaCO_3$ polymorphs within the pores driven by van der Waals force is quite difficult due to the movement of PO_4^{3-} ions in a very narrow space of the ICWMS adsorbent as indicated by its BET surface of 0.055 $m^2\ g^{-1}$ is very limited. The pattern of $[k_La]_d$ variation increased but that of $[k_La]_f$ variation decreased slowly with decreasing of the C_o/C_s ratio can be observed after passing from around 5% until reaching 100% of the PO_4^{3-} breakthrough. This indicates that the rate of adsorption depended on both FMT and PD ultimately controls the residence time of PO_4^{3-} uptake at the ICWMS-aqueous phase interface. The movement of PO_4^{3-} anions from DWTPE cannot enter the pores because the PO_4^{3-} anions would be repelled by the fixed coexisting Cl^-, NO_3^- and SO_4^{2-} anions inside the ICWMS adsorbent. The capacity of ICWMS material adsorbed the PO_4^{3-} ions from DWTPE can be increased by developing the pore space and acceptor sites of the ICWMS adsorbent by the various physical and chemical modifications. The modification of pore structure by the calcination process has been proposed to increase the BET surface of the WMS powder (Wei et al. 2018) giving an insight into the future development of the ICWMS adsorbent.

Conclusion

This study proposed the ICWMS material as a potential adsorbent for the adsorption of PO_4^{3-} from DWTPE applied in hydrodynamic column of the HPFCR treatment system. The performance of HPFCR to remove the pollutants of PO_4^{3-}, SS, COD and NH_4^+ from DWTPE reaches 98.7, 56.3, 37.5 and 9.5%, respectively, at 3.5 h of the experiment. The analysis of experimental data used the BDST, Thomas, and MMTF models enables to link the kinetic behaviors of PO_4^{3-} adsorption with the surface properties of ICWMS material gained from the EDXRF analysis, surfer analyser, SEM photographs, and XRD pattern. An application of the BDST models with its K_a and N_o values and Thomas models with its K_T and q_o values is limited to describe the detailed kinetic mechanisms of mass transfer controlled the overall adsorption rate of PO_4^{3-} onto ICWMS from DWTPE. The application of the MMTF models enables to describe the mechanisms of FMT and PD and determines the kinetic rate of PO_4^{3-} adsorption controlled by PD. The resistance of mass transfer for the adsorption of PO_4^{3-} ions onto ICWMS from DWTPE in hydrodynamic column was verified to contribute to the development of low-cost material as a potential adsorbent for the removal of PO_4^{3-} from aqueous solution in future.

Acknowledgements This research was supported by the Ministry of Higher Education, Malaysia, through Fundamental Research Grant Scheme Vote No. 4F956 and the Ton Duc Thang University Contract No. 307/2020/TĐT-HĐLV-NCV. The authors thank the Center for Environmental Sustainability and Water Security (IPASA) for laboratory facilities and the Indah Water Konsortium (IWK) Sdn. Bhd. for research collaboration.

Declarations

Conflict of interest All authors declare that they have no conflict of interest.

Ethical approval This article does not contain any studies with human participants or animals performed by any of the authors.

References

Abou Nohra JS, Madramootoo CA, Hendershot WH (2007) Modelling phosphate adsorption to the soil: Application of the non-ideal competitive adsorption model. Environ Pollut 149:1–9. https://doi.org/10.1016/j.envpol.2006.12.027

Afridi MN, Lee WH, Kim JO (2019) Effect of phosphate concentration, anions, heavy metals, and organic matter on phosphate adsorption

from wastewater using anodized iron oxide nanoflakes. Environ Res 171:428–436. https://doi.org/10.1016/j.envres.2019.01.055
Ahmed MJ, Hameed BH (2018) Removal of emerging pharmaceutical contaminants by adsorption in a fixed-bed column: A review. Ecotoxicol Environ Saf 149:257–266. https://doi.org/10.1016/j.ecoenv.2017.12.012
APHA (2017) Standard methods for the examination of water and wastewater, 23rd edn. American Public Health Association, Washington, DC
Bali M, Gueddari M (2019) Removal of phosphorus from secondary effluents using infiltration–percolation process. Appl Water Sci 9:54. https://doi.org/10.1007/s13201-019-0945-5
Bohart GS, Adams EQ (1920) Some aspects of the behavior of charcoal with respect to chlorine. J Am Chem Soc 42:523–544. https://doi.org/10.1021/ja01448a018
Boujelben N, Bouzid J, Elouear Z, Feki M, Jamoussi F, Montiel A (2008) Phosphorus removal from aqueous solution using iron coated natural and engineered sorbents. J Hazard Mater 151:103–110. https://doi.org/10.1016/j.jhazmat.2007.05.057
Bunce JT, Ndam E, Ofiteru ID, Moore A, Graham DW (2018) A Review of phosphorus removal technologies and their applicability to small-scale domestic wastewater treatment systems. Front Environ Sci 6:8. https://doi.org/10.3389/fenvs.2018.00008
Čadež V, Erceg I, Selmani A, Jurašin DD, Šegota S, Lyons DM, Kralj D, Sikirić MD (2018) Amorphous calcium phosphate formation and aggregation process revealed by light scattering techniques. Curr Comput-Aided Drug Des 8:254. https://doi.org/10.3390/cryst8060254
Charola S, Yadav R, Das P, Maiti S (2018) Fixed-bed adsorption of Reactive Orange 84 dye onto activated carbon prepared from empty cotton flower agro-waste. Sustain Environ Res 28:298–308. https://doi.org/10.1016/j.serj.2018.09.003
Crundwell FK (2017) On the mechanism of the dissolution of quartz and silica in aqueous solutions. ACS Omega 2:1116–1127. https://doi.org/10.1021/acsomega.7b00019
De Gisi S, Lofrano G, Grassi M, Notarnicola M (2016) Characteristics and adsorption capacities of low-cost sorbents for wastewater treatment: A review. Sustain Mater Technol 9:10–40. https://doi.org/10.1016/j.susmat.2016.06.002
de Sousa AF, Braga TP, Gomes ECC, Valentini A, Longhinotti E (2012) Adsorption of phosphate using mesoporous spheres containing iron and aluminum oxide. Chem Eng J 210:143–149. https://doi.org/10.1016/j.cej.2012.08.080
Fulazzaky MA (2011) Determining the resistance of mass transfer for adsorption of the surfactants onto granular activated carbons from hydrodynamic column. Chem Eng J 166:832–840. https://doi.org/10.1016/j.cej.2010.11.052
Fulazzaky MA (2013) Measurement of biochemical oxygen demand of the leachates. Environ Monit Assess 185:4721–4734. https://doi.org/10.1007/s10661-012-2899-z
Fulazzaky MA (2019) Study of the dispersion and specific interactions affected by chemical functions of the granular activated carbons. Environ Nanotechnol Monit Manage 12:100230. https://doi.org/10.1016/j.enmm.2019.100230
Fulazzaky MA, Khamidun MH, Din MFM, Yusoff ARM (2014a) Adsorption of phosphate from domestic wastewater treatment plant effluent onto the laterites in a hydrodynamic column. Chem Eng J 258:10–17. https://doi.org/10.1016/j.cej.2014.07.092
Fulazzaky MA, Salim NAA, Abdullah NH, Yusoff ARM, Paul E (2014b) Precipitation of iron-hydroxy-phosphate of added ferric iron from domestic wastewater by an alternating aerobic-anoxic process. Chem Eng J 253:291–297. https://doi.org/10.1016/j.cej.2014.05.049
Fulazzaky MA, Khamidun MH, Omar R (2013) Understanding of mass transfer resistance for the adsorption of solute onto porous material from the modified mass transfer factor models. Chem Eng J 228:1023–1029. https://doi.org/10.1016/j.cej.2013.05.100
Fulazzaky MA, Nuid M, Aris A, Muda K (2018) Mass transfer kinetics of biosorption of nitrogenous matter from palm oil mill effluent by aerobic granules in sequencing batch reactor. Environ Technol 39:2151–2161. https://doi.org/10.1080/09593330.2017.1351494
Jung KW, Hwang MJ, Ahn KH, Ok YS (2015) Kinetic study on phosphate removal from aqueous solution by biochar derived from peanut shell as renewable adsorptive media. Int J Environ Sci Technol 12:3363–3372. https://doi.org/10.1007/s13762-015-0766-5
Jurado I, Paese G, Schneider IH, Féris LA (2021) Phosphate removal from aqueous solutions using natural and thermic treated dolomites: equilibrium, kinetic, and thermodynamic. Int J Environ Sci Technol. https://doi.org/10.1007/s13762-021-03197-2
Karageorgiou K, Paschalis M, Anastassakis GN (2007) Removal of phosphate species from solution by adsorption onto calcite used as natural adsorbent. J Hazard Mater 139:447–452. https://doi.org/10.1016/j.jhazmat.2006.02.038
Karri RR, Sahu JN, Chimmiri V (2018) Critical review of abatement of ammonia from wastewater. J Mol Liq 261:21–31. https://doi.org/10.1016/j.molliq.2018.03.120
Kausar A, Bhatti HN, Iqbal M, Ashraf A (2017) Batch versus column modes for the adsorption of radioactive metal onto rice husk waste: Conditions optimization through response surface methodology. Water Sci Technol 76:1035–1043. https://doi.org/10.2166/wst.2017.220
Khadhri N, El Khames SM, Ben Mosbah M, Moussaoui Y (2019) Batch and continuous column adsorption of indigo carmine onto activated carbon derived from date palm petiole. J Environ Chem Eng 7:102775. https://doi.org/10.1016/j.jece.2018.11.020
Kim Y, Kim D, Kang SW, Ham YH, Choi JH, Hong YP, Ryoo KS (2018) Use of powdered cockle shell as a bio-sorbent material for phosphate removal from water. Bull Korean Chem Soc 39:1362–1367. https://doi.org/10.1002/bkcs.11606
Kumar RA, Velayudhan KT, Ramachandran V, Bhai RS, Unnikrishnan G, Vasu K (2010) Adsorption and removal kinetics of phosphonate from water using natural adsorbents. Water Environ Res 82:62–68. https://doi.org/10.2175/106143009x447939
Lalley J, Han C, Li X, Dionysiou DD, Nadagouda MN (2016) Phosphate adsorption using modified iron oxide-based sorbents in lake water: Kinetics, equilibrium, and column tests. Chem Eng J 284:1386–1396. https://doi.org/10.1016/j.cej.2015.08.114
Le Moigne FAC, Cisternas-Novoa C, Piontek J, Maßmig M, Engel A (2017) On the effect of low oxygen concentrations on bacterial degradation of sinking particles. Sci Rep 7:16722. https://doi.org/10.1038/s41598-017-16903-3
Li R, Wang JJ, Zhou B, Awasthi MK, Ali A, Zhang Z, Mahar A (2016) Enhancing phosphate adsorption by Mg/Al layered double hydroxide functionalized biochar with different Mg/Al ratios. Sci Total Environ 559:121–129. https://doi.org/10.1016/j.scitotenv.2016.03.151
Liu J, Jiang J, Aihemaiti A, Meng Y, Yang M, Xu Y, Chen X (2019) Removal of phosphate from aqueous solution using MgO-modified magnetic biochar derived from anaerobic digestion residue. J Environ Manage 250:109438. https://doi.org/10.1016/j.jenvman.2019.109438
Liu S, Sun Y, Wang R, Mishra SB, Duan H, Qu H (2018) Modification of sand with iron and copper derived from electroplating wastewater for efficient adsorption of phosphorus from aqueous solutions: A combinatorial approach for an effective waste minimization. J Clean Prod 200:471–477. https://doi.org/10.1016/j.jclepro.2018.07.254
Mekonnen DT, Alemayehu E, Lennartz B (2020) Removal of phosphate ions from aqueous solutions by adsorption onto leftover coal. Water 12:1381. https://doi.org/10.3390/w12051381

Mezenner NY, Bensmaili A (2009) Kinetics and thermodynamic study of phosphate adsorption on iron hydroxide-eggshell waste. Chem Eng J 147:87–96. https://doi.org/10.1016/j.cej.2008.06.024

Misra AK (2014) Climate change and challenges of water and food security. Int J Sustain Built Environ 3:153–165. https://doi.org/10.1016/j.ijsbe.2014.04.006

Nagoya S, Nakamichi S, Kawase Y (2019) Mechanisms of phosphate removal from aqueous solution by zero-valent iron: A novel kinetic model for electrostatic adsorption, surface complexation and precipitation of phosphate under oxic conditions. Separ Purif Technol 218:120–129. https://doi.org/10.1016/j.seppur.2019.02.042

Nakarmi A, Kim J, Toland A, Viswanathan T (2019) Novel reusable renewable resource-based iron oxides nanocomposites for removal and recovery of phosphate from contaminated waters. Int J Environ Sci Technol 16:4293–4302. https://doi.org/10.1007/s13762-018-2058-3

Osman NA, Ujang FA, Roslan AM, Ibrahim MF, Hassan MA (2020) The effect of palm oil mill effluent final discharge on the characteristics of *Pennisetum purpureum*. Sci Rep 10:6613. https://doi.org/10.1038/s41598-020-62815-0

Ovcharenko R, Voloshina E, Sauer J (2016) Water adsorption and O-defect formation on Fe_2O_3(0001) surfaces. Phys Chem Chem Phys 18:25560–25568. https://doi.org/10.1039/C6CP05313K

Passerini MD, Cunha-Santino MB, Bianchini I Jr (2016) Oxygen availability and temperature as driving forces for decomposition of aquatic macrophytes. Aquat Bot 130:1–10. https://doi.org/10.1016/j.aquabot.2015.12.003

Pember N, Millar GJ, Couperthwaite SJ, De Bruyn M, Nuttall K (2016) BDST modelling of sodium ion exchange column behaviour with strong acid cation resin in relation to coal seam water treatment. J Environ Chem Eng 4:2216–2224. https://doi.org/10.1016/j.jece.2016.04.002

Podder MS, Majumder CB (2016) Fixed-bed column study for As(III) and As(V) removal and recovery by bacterial cells immobilized on Sawdust/$MnFe_2O_4$ composite. Biochem Eng J 105:114–135. https://doi.org/10.1016/j.bej.2015.09.008

Recepoğlu YK, Kabay N, Ipek IY, Arda M, Yüksel M, Yoshizuka K, Nishihama S (2018) Packed bed column dynamic study for boron removal from geothermal brine by a chelating fiber and breakthrough curve analysis by using mathematical models. Desalination 437:1–6. https://doi.org/10.1016/j.desal.2018.02.022

Riahi K, Chaabane S, Thayer BB (2017) A kinetic modeling study of phosphate adsorption onto *Phoenix dactylifera* L. date palm fibers in batch mode. J Saudi Chem Soc 21:S143–S152. https://doi.org/10.1016/j.jscs.2013.11.007

Sabeen AH, Ngadi N, Noor ZZ, Raheem AB, Agouillal F, Mohammed AA, Abdulkarim BI (2018) Characteristics of the effluent wastewater in sewage treatment plants of Malaysian urban areas. Chem Eng Trans 63:691–696. https://doi.org/10.3303/CET1863116

Salim NAA, Fulazzaky MA, Puteh MH, Khamidun MH, Yusoff ARM, Abdullah NH, Ahmad N, Lazim ZM, Maria Nuid M (2021) Adsorption of phosphate from aqueous solution onto iron-coated waste mussel shell: Physicochemical characteristics, kinetic, and isotherm studies. Biointerface Res Appl Chem 11:12831–12842

Silva M, Baltrusaitis J (2020) A review of phosphate adsorption on Mg-containing materials: kinetics, equilibrium, and mechanistic insights. Environ Sci: Water Res Technol 6:3178–3194. https://doi.org/10.1039/D0EW00679C

Song X, Pan Y, Wu Q, Cheng Z, Ma W (2011) Phosphate removal from aqueous solutions by adsorption using ferric sludge. Desalination 280:384–390. https://doi.org/10.1016/j.desal.2011.07.028

Syafiuddin A, Salmiati S, Jonbi J, Fulazzaky MA (2018) Application of the kinetic and isotherm models for better understanding of the behaviors of silver nanoparticles adsorption onto different adsorbents. J Environ Manage 218:59–70. https://doi.org/10.1016/j.jenvman.2018.03.066

Tomei MC, Stazi V, Daneshgar S, Capodaglio AG (2020) Holistic approach to phosphorus recovery from urban wastewater: Enhanced biological removal combined with precipitation. Sustainability 12:575. https://doi.org/10.3390/su12020575

Torit J, Phihusut D (2019) Phosphorus removal from wastewater using eggshell ash. Environ Sci Pollut Res 26:34101–34109. https://doi.org/10.1007/s11356-018-3305-3

Wei D, Zhang H, Cai L, Guo J, Wang Y, Ji L, Song W (2018) Calcined mussel shell powder (CMSP) via modification with surfactants: Application for antistatic oil-removal. Mater 11:1410. https://doi.org/10.3390/ma11081410

Wu K, Li Y, Liu T, Huang Q, Yang S, Wang W, Jin P (2019) The simultaneous adsorption of nitrate and phosphate by an organic-modified aluminum-manganese bimetal oxide: Adsorption properties and mechanisms. Appl Surf Sci 478:539–551. https://doi.org/10.1016/j.apsusc.2019.01.194

Zhang Z, Yan L, Yu H, Yan T, Li X (2019) Adsorption of phosphate from aqueous solution by vegetable biochar/layered double oxides: Fast removal and mechanistic studies. Bioresour Technol 284:65–71. https://doi.org/10.1016/j.biortech.2019.03.113

Zhong Z, Yu G, Mo W, Zhang C, Huang H, Li S, Zhu H (2019) Enhanced phosphate sequestration by Fe(III) modified biochar derived from coconut shell. RSC Adv 9:10425–10436. https://doi.org/10.1039/c8ra10400j